Mon. Not. R. Astron. Soc. **349,** 1365–1380 (2004) doi:10.1111/j.1365-2966.2004.07609.x

Contaminants in ATCA baselines with shadowing: a case study of cross-talk in short-spacing interferometers

Ravi Subrahmanyan[1]★ and Avinash A. Deshpande[1,2,3]

[1]*Australia Telescope National Facility, CSIRO, Locked bag 194, Narrabri, NSW 2390, Australia*
[2]*Raman Research Institute, Sadashivanagar, Bangalore 560 080, India*
[3]*Arecibo Observatory, NAIC, HC3 53995, Arecibo, PR 00612, USA*

Accepted 2004 January 9. Received 2003 October 7; in original form 2003 April 10

ABSTRACT

Interferometric telescopes made of close-packed antenna elements are an important tool for imaging extended radio sources, specifically structures that have angular sizes comparable to or even greater than the full width at half maximum of the beams of the antennas. They have proved useful in observations of cosmic microwave background anisotropies that require high brightness sensitivity. However, the visibilities measured in baselines formed between close antenna elements – in particular, between shadowed elements – of Fourier-synthesis arrays are often observed to be corrupted. We discuss the multiplicative and additive errors affecting such short-baseline interferometers.

As a case study, we have examined the nature of the spurious correlations between the Cassegrain-type paraboloidal reflectors that are elements of the Australia Telescope Compact Array. In configurations with geometric shadowing, the cross-talk here appears as an additive component. Analysis of the characteristics of this cross-talk leads us to believe that when these reflector antennas are in a shadowed configuration, the receivers in the antenna pair pick up correlated emission from opposite sides of the main reflector surface of the front antenna. The slots between the panels that make up the main reflector surface provide the pathway for the coupling across the reflector surface. This mode of cross-talk may be avoided by constructing the main reflectors of short-spacing interferometers as continuous conducting surfaces.

Key words: atmospheric effects – instrumentation: interferometers – techniques: interferometric – telescopes – cosmic microwave background – cosmology: observations.

1 INTRODUCTION

The techniques of radio interferometry and Fourier synthesis arrays for imaging have developed remarkably since the first synthesis images were constructed by Ryle, Hewish & Shakeshaft (1959) and Earth-rotation Fourier synthesis was described by Ryle (1962) more than four decades ago. Today, large-aperture synthesis arrays of precision paraboloidal reflectors like, for example, the Very Large Array, the Very Long Baseline Array, the Australia Telescope Compact Array (ATCA) and the Westerbork Synthesis Radio Telescope routinely provide astronomers with visibility measurements with which high-resolution and high-dynamic-range radio images of celestial objects are synthesized. The quest for extreme angular resolution has led to the development of Very Long Baseline Interferometry in space which involves antennas separated by distances exceeding the diameter of the Earth.

For years, conventional wisdom argued against using interferometers for observations which required high surface brightness sensitivity; total-power measurements with single-dish telescopes were the preferred option. The reason is that interferometers are 'correlated-flux-sensitive' telescopes which respond well to discrete 'point sources'; they do not respond to the uniform sky background and couple poorly to extended emission that is 'resolved' by the interferometer spacing. For example, prior to 1990, all successful attempts to detect the Sunyaev–Zeldovich effect (SZE; Sunyaev & Zeldovich 1972) towards clusters of galaxies were made with single-dish telescopes (see, for example, the compilation in Birkinshaw 1990). However, this conviction has changed in the last decade: the advantages of interferometry and Fourier synthesis – its inherent ability to provide significant rejection of any contributions from the atmosphere and ground and the stability in its measurements – are often perceived to outweigh the disadvantages. Interferometers formed between closely spaced elements provide visibility measurements of extended structure and, with recent improvements in receiver technology which allow low-noise amplifiers and compact cryogenics, it is now possible to construct useful interferometers of small aperture elements and with short baselines. Indeed, today we have Fourier-synthesis images of the SZE towards several tens

★E-mail: rsubrahm@atnf.csiro.au

of clusters (see, for example, Jones et al. 1993; Carlstrom et al. 2000).

The quest for high brightness sensitivity and the scientific motivations for imaging extended low-surface-brightness features in the sky have pushed telescope designers towards arrays of small-sized elements in ultracompact configurations. An example of such a goal is the imaging of temperature variations in the cosmic microwave background (CMB): on large angular scales the anisotropies are believed to be the imprint of primordial density perturbations and on smaller angular scales they are due to the propagation of the relic photons through the extended gaseous coronae of galaxy clusters and diffuse hot intergalactic gas. The signals are extremely weak: the primary CMB anisotropy is a few tens of μK, and the polarized CMB anisotropy is expected to be a few μK. These are a tiny fraction of the telescope system temperature and a very important design consideration is the control and rejection of spurious systematics. These key astrophysical questions are being probed today by a small but growing number of 'special-purpose' aperture synthesis telescopes which have been built using elements of small-diameter apertures. These ground-based telescopes are imaging the CMB anisotropies with poor angular resolutions/scales of about a degree.

Interferometric imaging via Earth-rotation Fourier synthesis has the added advantage that the 'fringe filtering' provides rejection against systematics that do not have the same fringe rate as that for the celestial signal of interest. Consequently, it is advantageous if the antenna elements forming the interferometric telescope are not comounted (on a platform) but are independently mounted. The downside of such an approach is that the antenna elements run the risk of shadowing when the portion of the wavefront incident on an antenna element aperture is blocked along the path by parts of the aperture of another antenna element located adjacent and in front. The visibilities measured by an interferometer pair in a shadowed configuration, or in a situation where the projected element apertures are close to shadowing, are usually corrupted. However, it is these very baselines between apertures with close projected spacings that provide the highest sensitivity to large angular scale variations in sky surface brightness temperature.

To avoid shadowing in small arrays, a comounted array design may be preferred. However, these arrays in which the apertures are fixed to a platform will be more susceptible to spurious pickups; consequently, they entail an investment of considerable effort towards the development of appropriate calibration strategies to subtract the unwanted additive contributions, particularly those local to the platform (see Subrahmanyan 2002, for an alternative viewpoint). Making choices in the design of ultracompact arrays requires understanding the trade-offs: an important aspect is understanding the magnitude and the origin of spurious contributions that arise between closely spaced antennas.

The next-generation radio telescopes, like the Atacama Large Millimeter Array, Allan Telescope Array and the Square Kilometre Array, which are to have large total collecting areas for high sensitivity, are being designed to be arrays of small elements. The arrays would have closely spaced interferometers for wide-field imaging of extended emission. Because short-spacing interferometers are important for recovering low spatial frequencies (sometimes using mosaicing techniques), understanding the causes for spurious contaminants in the visibility measurements made using closely spaced elements is important for designing these next-generation arrays.

In this paper, we examine the nature of the spurious signals that are observed in those short-spacing interferometers of the ATCA when there is geometric shadowing. We begin in Section 2 by listing the different mechanisms that corrupt visibility measurements made using short-spacing interferometers. Observations of spurious visibilities in baselines between ATCA antennas in which one element shadows the other is described in Section 3; later sections describe investigations into the nature of this unwanted cross-talk.

2 THE ERRORS IN INTERFEROMETER BASELINES WITH GEOMETRIC SHADOWING

In an interferometer that is formed between antenna elements which are identical and spaced well apart, the measured visibility may be described as an integral over the product of

(i) the sky brightness distribution,
(ii) the primary beam pattern of the antenna elements, and
(iii) the interferometer (angular) pattern that is determined by the projected antenna spacing or baseline.

In the visibility domain, the spatial frequency range that is sampled by the measured visibility on a baseline is determined by the aperture illuminations of the two antenna elements and the projected interferometer spacing. In interferometer arrays, closely spaced antenna elements that are independently mounted would shadow each other when the projected baseline is shorter than the average physical extent of the two apertures viewed along the baseline, a situation encountered when observing in particular azimuth/elevation (AZ/EL) zones. Shadowing causes the measured visibilities to differ from that expected based on the above integral and the calibration of the measurements may suffer.

Some of the possible multiplicative errors in these visibility measurements are listed below; a few of these assume that the array elements are reflector-type antennas.

(i) The presence of the shadowing antenna element in front of the shadowed antenna distorts the far-field antenna radiation pattern corresponding to the shadowed antenna. The blocking of the aperture of the shadowed antenna reduces its effective collecting area. If we consider baselines between a shadowed antenna and any other array element that is unblocked, these interferometers may be considered to be formed between a pair non-identical apertures. The effective primary beam pattern in an interferometer is the geometric mean of the individual element antenna patterns and, therefore, in the geometric optics (GO) approximation the effective primary beam for the case where the aperture of one element is shadowed may be computed from (the Fourier transform of) the convolution of the illuminations corresponding to the partially blocked aperture with an unblocked aperture. This convolution defines the weighting, in the visibility domain, for the integral that yields the visibility measurement on the baseline between the elements.

(ii) The 'effective' baseline to the shadowed antenna is modified and may vary also with the extent of shadowing: the interferometer (or array) pattern for baselines to the shadowed antenna will vary with the shadowing geometry.

(iii) The system temperature of the shadowed antenna may be elevated because there may be absorbing elements in the backup structure of the antenna in front (which emit with a brightness corresponding to the ambient temperature) and/or the shadowed antenna may now pick up ground emission reflected off the structure of the antenna in front.

(iv) Diffraction and scattering will occur at the edge of the antenna in front and these imply that the wavefront is no longer planar as it arrives at the aperture of the shadowed antenna. This necessitates a physical optics (PO) treatment of the blocking.

The above list was of multiplicative distortions/errors in the measured visibility. There would also be spurious additive errors, some of which are listed below.

(i) The coupling between the aperture fields of two nearby apertures (see, for example, Padin et al. 2000) would result in receiver noise, which radiates out into the aperture of one element, to be coupled to the aperture of any adjacent element. Receiver noise may also leak between close antennas as a result of coupling pathways created by scattering off structural elements like, for example, subreflector support structures. Coupling paths may also exist as a result of transmission through the main reflector surface if this surface is not perfectly reflecting/opaque at the observing frequency. The main reflector may be porous because the surface might be a mesh, or because the reflector panels might have holes to reduce wind loading, or because the main reflector might be constructed from solid panels and there might be slots between the panels.

(ii) The short baseline may respond to the near-field atmospheric emission in overlapping near-field radiation patterns. In the case of antennas with small apertures and operating at large wavelengths, the transition from near to far field may occur within the atmosphere: consequently, emission from the atmosphere in overlapping far-field patterns may not be rejected by the interferometer. These effects have been examined by Church (1995) and Lay & Halverson (2000).

(iii) The short-spacing interferometer may respond to nearby environmental emission in overlapping spill-over patterns on the ground. Variations in brightness temperature across the ground and because of trees or buildings would be the cause of a 'ground fringe'.

(iv) Any interferometer that has a baseline component perpendicular to the horizon may respond to the discontinuity in brightness at the horizon between the sky and ground, if both the antennas respond to the interface.

(v) Shadowing and overlap between projected apertures may, effectively, generate a zero-spacing interferometer that responds to the uniform sky, atmosphere and ground.

Some of the above-mentioned items are not independent and reflect simply different viewpoints of the same phenomenon.

Besides these problems, it may also be mentioned here that external interference is of greater deleterious consequence for short-spacing interferometers because the associated fringe rate is small. Additionally, because the effects of bandwidth and time-averaging smearing are smaller for short baselines, strong sources (like the Sun) may produce a correlated response even if they are at large angles from the antenna pointing direction.

Correction for some of the multiplicative effects will vary across the primary beam. In the celestial sphere, the primary beam may be time-varying as a source is tracked across the sky if the effective aperture illumination of the shadowed antenna changes as a result of changes in the degree of geometric shadowing. Equivalently, in the spatial frequency (visibility) domain, the measured visibility is an average over a region of the spatial-frequency plane with a time-varying weighting function.

3 OBSERVATIONS OF THE CROSS-TALK BETWEEN ATCA ANTENNAS

The ATCA is an array of Cassegrain-type antennas with shaped reflectors and forms a Fourier-synthesis radio telescope. Five antennas, labelled ca01–ca05, are moveable along a 3 km east–west railtrack – which also has a short north–south spur – and may be sited at any one of several fixed station locations along the track. The main reflectors of the antennas are 22 m in diameter and the minimum allowed baseline is 30.6 m. All the cross-talk measurements described below were made between a pair of antennas located on stations that were 30.6 m apart on the east–west track.

The Cassegrain antennas have a short focal ratio, with an f/D ratio of 0.32, and have axially symmetric optics. A 2.74-m diameter subreflector is mounted on a tetrapod above the 22-m diameter main reflector. The reflector optics are 'shaped' to maximize G/T: the ratio of the antenna gain to the antenna system temperature; therefore, the main and subreflector surfaces depart from paraboloidal and hyperboloidal. The subreflector is made of solid aluminium; the main reflector surface is formed by six concentric rings of panels. Originally, the inner four rings out to 5.865-m radius were made of solid panels and the outer two rings were made of perforated panels; recently, as part of a 'high-frequency upgrade' of the telescope, the outer rings have been replaced with solid panels. The panels are constructed from segments that are bonded to stretch-formed ribs of 'I' section aluminium; rivets connect these panel sections to the ribs. The backup structure supporting the panels is an open truss system. The antenna mount is alt-AZ.

Most measurements described in this section were made at 3- and 6-cm wavelengths. The feed, whose frequency range spans both these wavelength bands, is a wide-band compact corrugated horn at the Cassegrain focus. The feed is followed by an ortho-mode transducer which provides dual linear polarization signals, labelled X and Y, which are down-converted and used by the correlator to compute the correlation on any given baseline. When the antenna is viewed from the front (face on), the legs of the tetrapod, which support the subreflector, are oriented along 0° and 90° position angle (PA) and the two orthogonal linear feeds may be visualized as picking up the X and Y polarization electric field components at 45° and 135° PA respectively. The phase difference between the two linear polarization signal paths in any antenna is measured by its on-line injected-noise calibration system and the four cross-correlation products $X_1X_2^*$, $Y_1Y_2^*$, $X_1Y_2^*$ and $Y_1X_2^*$ (denoted hereafter by XX, YY, XY and YX, respectively) between any antenna pair may be converted to Stokes parameter correlations. The measurements were made using 128-MHz bandwidths centred at 8640 MHz in the 3-cm band and at 4800 MHz in the 6-cm band. The ATCA correlator measures correlation coefficients over a range of positive and negative lags and the measurements are then Fourier transformed to provide visibility measurements over a set of frequency channels covering the observing band. The data described here were acquired in 16 independent 8-MHz channels covering the 128-MHz bands.

3.1 The observed visibilities in baselines with shadowing

The 'unresolved' continuum source B1741−038 was observed over the HA range +1 to +5 h till before the source set in the west; during this time the source elevation decreased from 60° to 15°. Visibility data were acquired using three ATCA antennas – ca01, ca02 and ca03 – configured on the east–west track so that ca01 and ca02 were separated by 30.6 m and ca03 was located 400 m down the track to the west. The array configuration is depicted in Fig. 1. Before and as the source set, antenna ca02 progressively shadowed ca01; ca03 did not at any time block the aperture of ca02 and, consequently, ca02 and ca03 remained unblocked throughout.

The observed visibility amplitudes at 4800 MHz, calibrated in flux density and expressed in units of janskies (Jy), are shown in Fig. 2. It may be noted here that the visibilities have been corrected for changes in the system temperatures of the antennas (related mostly to changes in antenna elevation and shadowing). The panels show the Stokes I, Q, U and V parameter amplitudes on the

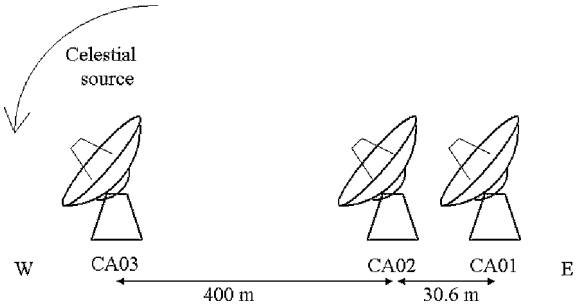

Figure 1. The array configuration for the observations described in Section 3.

baselines ca03–ca01 and ca02–ca01 versus the length of the projected baseline ca02–ca01. When the projected antenna separation, on the ca02–ca01 baseline, is less than the dish diameter (i.e. 22 m), ca02 geometrically shadows ca01. The drop in the visibility amplitude on the ca03–ca01 baseline, as antenna ca01 is increasingly shadowed by ca02, is because the effective collecting area of ca01 is reduced when it is shadowed and the amplitude change may be considered to be an 'antenna-dependent' effect. All unshadowed antennas in the array would show a similar drop in visibility amplitude in baselines with the shadowed antenna ca01. The behaviour of the amplitudes on the ca02–ca01 baseline is observed to be unlike that seen in the ca03–ca01 baseline: coincident with the onset of geometric shadowing (when the projected separation reduces below 22 m), the Stokes *I*, *Q* and *U* amplitudes on the ca02–ca01 baseline are observed to diverge from the ca03–ca01 amplitude and the difference grows as the degree of shadowing increases. No significant flux density is observed in Stokes *V* either before or after the onset of geometric shadowing. We believe that the divergence in the Stokes *I*, *Q* and *U* amplitudes in the short-baseline interferometer ca02–ca01 is because of an additive 'baseline-dependent' component that is observed in the baseline between the shadowing and shadowed antennas; we hereinafter refer to this spurious correlated signal component as cross-talk.

3.2 Spurious additive visibilities on shadowed baselines

We have examined the additive cross-talk, in isolation, by observing towards a 'blank' sky region with a pair of antennas in a situation where one antenna shadows the other. Using antennas ca01 and ca02, separated by 30.6 m on the east–west track, a blank field at -4° declination (identical to that of the source B1741−038) was observed as the field set in the west and the western antenna, ca02, increasingly shadowed ca01 which was located to its east on the railtrack. The observed visibility amplitudes and phases at 4800 MHz versus the projected antenna separation are shown in Fig. 3. Cross-talk was observed in the ca02–ca01 baseline when the projected separation was less than the dish diameter (22 m) and the antenna in front, ca02, geometrically shadowed the antenna at the back, ca01. The Stokes *I* amplitude of the cross-talk progressively increased as the geometric shadowing increased and the projected baseline reduced; the Stokes *I* cross-talk phase is fairly constant in the shadowed regime. The linearly polarized Stokes *Q* and *U* amplitudes are, at 4800 MHz, about 20 per cent of the Stokes *I* amplitude; however, the polarization Stokes parameter amplitudes do not have a monotonic behaviour with increasing shadowing and their phases vary with the geometry of the shadowing. A small Stokes *V* component is also detected at 4800 MHz, which is about 5 per cent of the Stokes *I* amplitude.

In an attempt to correct the visibility on the short-baseline ca02–ca01 for the additive cross-talk, the complex cross-talk visibility

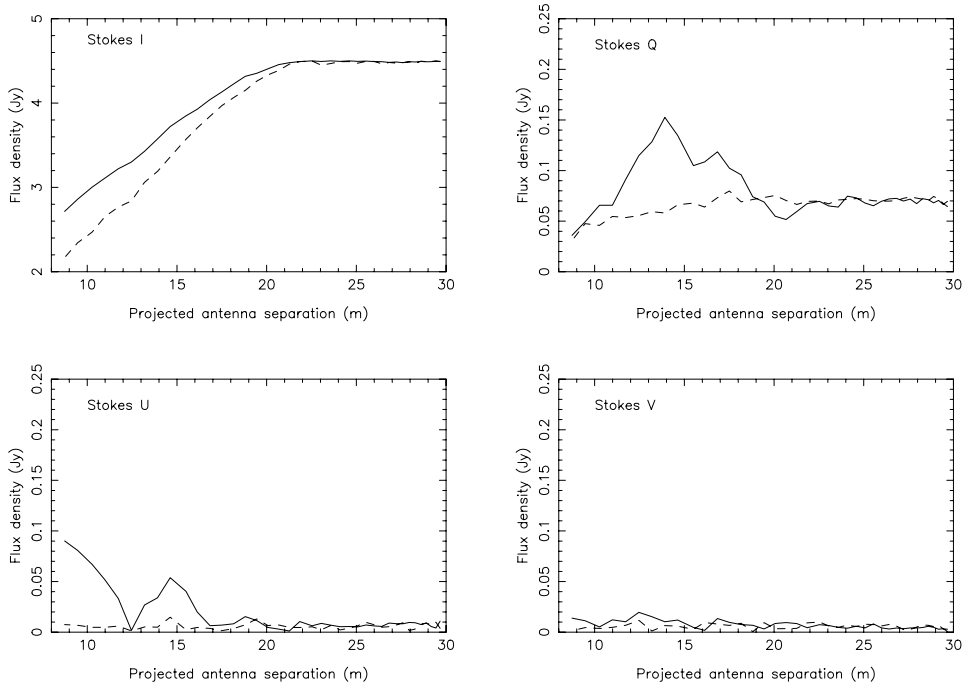

Figure 2. Effects of shadowing on visibilities of a continuum unresolved source. The panels show Stokes *I*, *Q*, *U* and *V* visibility amplitudes at 4800 MHz. The data are plotted as a function of the projected spacing between ca01 and ca02; geometric shadowing of ca01 begins when this projected antenna separation falls below 22 m. The amplitudes on the baseline between the shadowed antenna (ca01) and the shadowing antenna (ca02) are shown using continuous lines and those between the shadowed antenna (ca01) and a distant antenna (ca03) are shown using dashed lines. Note that the flux density scale runs from 2 to 5 Jy for the panel showing the Stokes *I* amplitudes whereas the scale runs over the range 0 to 0.25 Jy in the panels showing the other Stokes parameter amplitudes.

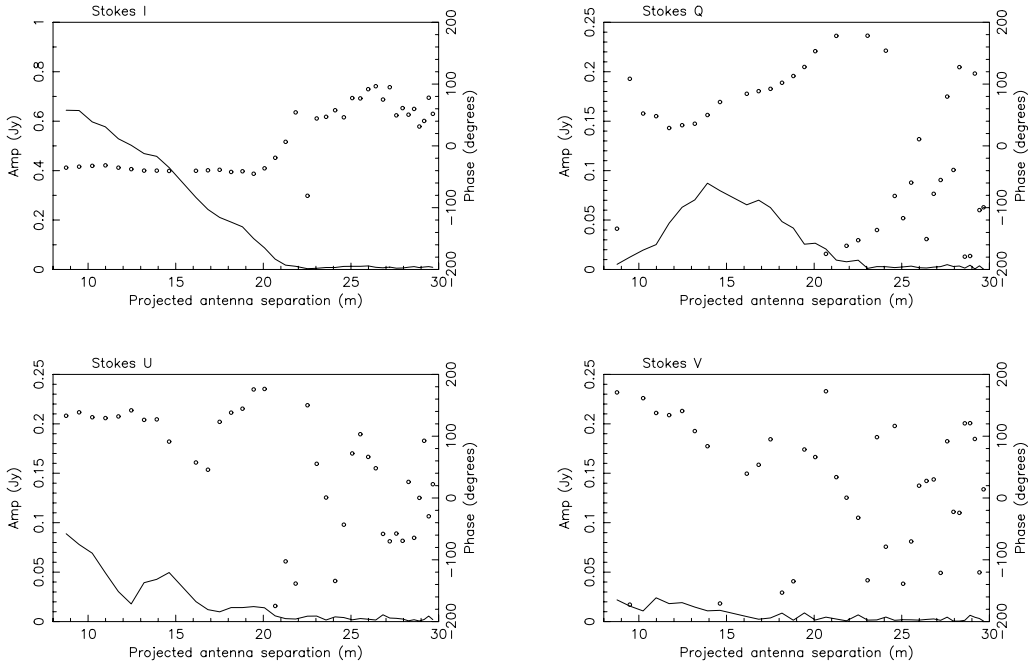

Figure 3. Cross-talk visibilities – observed on the ca02–ca01 baseline – versus the projected antenna spacing in metres. The four panels show the cross-talk in the four Stokes parameters, the amplitudes are plotted as continuous lines and the phases are shown using symbols. Note that the vertical scale runs from 0 to 1 for Stokes *I* and runs over the range 0–0.25 in the panels showing the other Stokes parameters. The onset of geometric shadowing occurs at 22 m.

observed on the blank field were subtracted (vectorially) from the visibilities observed on the calibrator source at the same geometric shadowing. Following the subtraction of the additive cross-talk, the ca02–ca01 baseline would be expected to have only antenna-based errors associated with the blockage of the aperture of ca01 and these multiplicative errors would be the same as those afflicting the ca03–ca01 baseline. The subtraction was successful within the errors in the measurements: the corrected ca02–ca01 visibilities in all four Stokes parameters were observed to have a behaviour similar to those on the ca03–ca01 baseline.

It is remarkable that the complex spurious signal observed towards the blank field (Fig. 3), in all four Stokes parameters, is the same as the additive cross-talk component present in the observations of the unresolved source (Fig. 2). The inference is that the cross-talk is not a coupling of the incident power, from the source(s) at the field centre, via a new path which is created because of shadowing. The cross-talk is a complex additive (and not a multiplicative) error on the short baseline in each of the Stokes parameters, it has a high degree of linear polarization, and the cross-talk amplitude and phase depend on the shadowing geometry.

4 CHARACTERIZATION OF THE CROSS-TALK

The additive cross-talk is observed, using the ATCA spectral line correlator, to be a continuum signal and not a narrow-band line. The cross-talk originates as broad-band noise and is not, for example, a local oscillator or any such tone-like signal generated in the receiver electronics.

With a pair of antennas in a shadowed configuration, both antennas pointing towards the same direction and with the geometric delay compensated for the antenna pointing centre, we have observed the cross-talk with a 128-MHz bandwidth and examined the lag-spectrum with 3.9-ns steps and over a ± 125-ns range. The cross-talk appears at 'zero' lag, i.e. with a delay appropriate for a continuum source at the antenna-pointing centre. From the lack of any detectable phase gradient across the 128-MHz band, we infer that the cross-talk appears to be coupling into the signal paths of the adjacent antennas with a delay that is the same as the geometric delay within ±0.3 ns (corresponding to a free-space propagation path difference of less than 10 cm). We have examined the cross-talk phase in widely separated observing bands and observed that the phase has a complex and slow variation with frequency. The total phase change is about 2π radians over the range 1384–9152 MHz. The observed phase variation with frequency is consistent with a small difference between the geometric delay and the relative delays between the cross-talk signal paths to the two antennas; the observations imply that this delay path difference is at most several centimetres. Operating the receivers in a spectral-line mode and with a narrow bandwidth, we have examined the correlation between the antenna signals over a range ±128 μs about the geometric delay and do not see any other signal over this large range.

The amplitude of the cross-talk signal decreases with increasing frequency: in the range 1384–8640 MHz, the amplitude, calibrated in Jy, roughly decreases as $S_\nu \propto \nu^{-1}$, where ν is the observing frequency. The cross-talk has an equivalent antenna temperature which also decreases as $T_a \propto \nu^{-1}$. At centimetre wavelengths, the cross-talk is observed at a level corresponding to a correlation coefficient of about 0.1 per cent and the amplitude corresponds to a geometric mean antenna temperature of about 50 mK.

The observed cross-talk amplitude and phase remain unchanged when the noise diodes, which inject noise for calibrating the receiver gain and system temperature, are switched off; this is a confirmation that the calibration noise diodes are not the source of the power for the 'unwanted' correlation.

The cross-talk signal appears as if it originates in the sky from the antenna-pointing direction and with a delay appropriate for signals from that sky direction. Therefore, we believe that the cross-talk

is not due to the direct coupling of common ground radiation into the two receivers. Additionally, we do not believe that the spurious correlation is because of any leakage of receiver noise from the front antenna and into the signal path of the antenna behind.

The cross-talk is because of a common mode signal that enters the two receivers located in the adjacent antennas. The sharpness of the response in the lag domain argues in favour of a dominant and perhaps a single coupling path and against a scenario where the coupling is via multiple scattering paths, unless these multiple paths have the same differential delays. Coupling because of scattering off, for example, the subreflector support structures may be expected to be spread over a range of delays.

4.1 Dependence of the cross-talk amplitude on the shadowing configuration

As the projected baseline between a pair of ATCA antennas decreases to values below the antenna diameter, cross-talk is observed and the Stokes *I* amplitude of the cross-talk increases as the projected baseline reduces further. With two antennas on stations separated by the minimum spacing of 30.6 m on the east–west track, geometric shadowing would be a maximum (and the projected baseline would be a minimum) when the antennas are pointed along the track towards AZ of 90° or 270° and the antenna elevations are at their lowest; the cross-talk amplitude in Stokes *I* is observed to decrease systematically away from these sky positions. We observed the cross-talk amplitudes when the 30.6-m baseline interferometer was pointed towards a mosaic of AZ–EL positions in the range AZ: 220°–320° and EL: 15°–55°. The variation in the Stokes *I* cross-talk amplitude, as well as in the *XX* and *YY* polarization products, versus offsets in the pointing from AZ 270° and EL 0°, is shown in Fig. 4.

When the projected baseline exceeds the antenna diameter and there is no geometric shadowing, the cross-talk amplitude in Stokes *I* as well as in the *XX* and *YY* polarizations drop to zero (or below our detectability).

The Stokes *I* cross-talk amplitude across the ranges of azimuth and elevation offsets is observed to have a circular symmetry about the direction of complete shadowing: it is thus dependent only on the length of the projected shadowed baseline and independent of the position angle of the projected baseline. The symmetry adds weight to the argument against ground radiation as a source of the cross-talk.

The *XX* and *YY* polarization products show different azimuth–elevation dependences that depart from such circular symmetry: the cross-talk is linearly polarized with *XX* cross-talk amplitude exceeding the *YY* amplitude for positive azimuthal offsets and vice versa. This implies that when a pair of antennas, which are in a shadowed configuration, are viewed face on and from along their pointing direction, the net cross-talk at 4800 MHz is partially linearly polarized and has an equivalent net *E*-field that appears as if it is oriented perpendicular to the line joining their centres.

The variation in the cross-talk amplitude on a 30.6-m baseline is shown in Fig. 5 versus the length of the projected baseline. These data were obtained at 4800 MHz. As noted earlier, the cross-talk signal is significant only when the antennas geometrically shadow and the projected baseline length drops below 22 m. We have plotted, in the same figure, the area of geometric shadowing (the area of the overlap segment) versus the projected baseline using a dotted line. Also plotted (using a dashed line) is the length of the rim of the front antenna, which appears across the aperture of the back antenna, when the antennas in a shadowed configuration are viewed face on and from along their pointing direction. The comparison indicates that the cross-talk arises owing to a coupling associated with the area of geometric shadowing; however, the effect is not uniform and, at least at 4800 MHz, is biased towards the outer edge of the overlap segment.

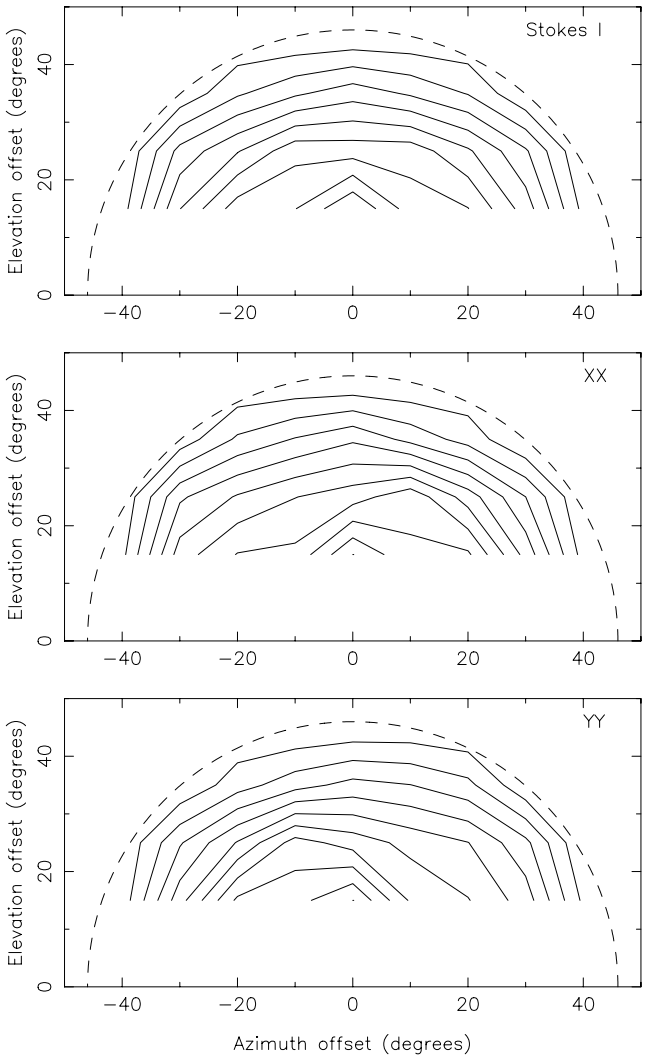

Figure 4. Contours of the cross-talk amplitude at 4800 MHz: the upper panel shows the Stokes *I* amplitude, the lower left panel is for the *XX* polarization and the lower right panel is of the *YY* polarization amplitude. The axes represent the offset in pointing direction from 0° EL and 270° AZ. The maximum cross-talk amplitude was observed at an AZ of 270° when the antennas were at their lower EL limit of 15°; contours are shown at intervals of 10 per cent of this maximum amplitude. Geometric shadowing occurs for offsets within the dashed circle and no significant cross-talk amplitude is observed when the offsets cause the pointing to lie outside this circle.

5 THE DISTRIBUTION OF THE CROSS-TALK ACROSS THE APERTURES

The cross-talk is because of an 'unwanted' signal that enters the receivers of the antennas, which are in a configuration where one of them geometrically shadows the other. The interferometer response is because of coherence between these signals at the two antennas: it may be noted here that the interferometer response does not

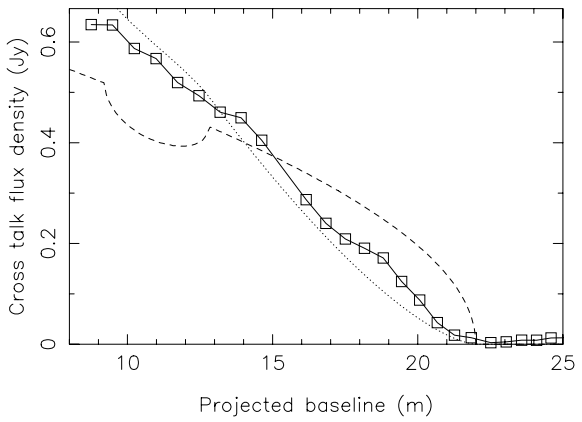

Figure 5. As the projected baseline between two antennas that are in a shadowed configuration decreases, the observed cross-talk amplitude (shown as a continuous line joining the box symbols) is compared with the area of the back antenna that is geometrically shadowed (dotted line) and the length of the rim of the front antenna that appears projected on the back antenna aperture (dashed line). The observed cross-talk amplitudes displayed are at 4800 MHz; the vertical scales for the rim length and shadowing area are arbitrary.

require a spatial coherence within the individual apertures, it only requires that there be coherence between the fields incident on the two apertures. The radiation field that causes the cross-talk would have a distribution across the apertures of the two antennas and examining these distributions is important to understanding the source of the cross-talk and the nature of its coupling into the two signal paths. When an incident electromagnetic wave is spatially coherent across the space containing a pair of antennas, the spatial distribution of the field which couples into the individual antennas may be measured using standard holographic methods (Bennett et al. 1976; Scott & Ryle 1977). The cross-talk we observe at the ATCA in shadowed configurations may not be due to a wavefront having transverse spatial coherence. However, it should be still possible to seek the equivalent aperture plane distributions of the cross-talk signal through holographic reconstruction if the signal couples into the aperture planes of the antennas in a distributed manner.

5.1 One-dimensional analysis of the distribution in the cross-talk

A pair of antennas were configured 30.6 m apart on the east–west track and pointed along the track at AZ 270° and EL 20°. Geometric path delays and phases were compensated for this sky direction. In this shadowed configuration, a cross-talk signal is observed. Keeping one of the two antennas fixed on the above pointing, the other antenna pointing was varied to scan across a range of offsets in azimuth and elevation around the nominal pointing direction and the complex cross-talk visibility were recorded. In Figs 6 and 7 we show the variation in the cross-talk amplitude and phase at 4800 MHz as a function of the offset from the nominal pointing direction (AZ 270°; EL = 20°); Fig. 6 shows the visibility variations for pointing offsets in azimuth and Fig. 7 displays these for elevation offsets from the nominal position. In each of these figures, the panels on the left represent the case where the pointing of the antenna at the back was kept fixed at the nominal position while the antenna in front executed the scan patterns; the panels on the right are for the case where the antenna in front had its pointing fixed towards the nominal direction while the antenna behind executed the scans in azimuth and elevation. For each of these cases, the measured Stokes *I* visibilities as well as the *XX* and *YY* polarization products are shown in separate panels. The visibility phases shown in the figures represent the phase of the scanning antenna with respect

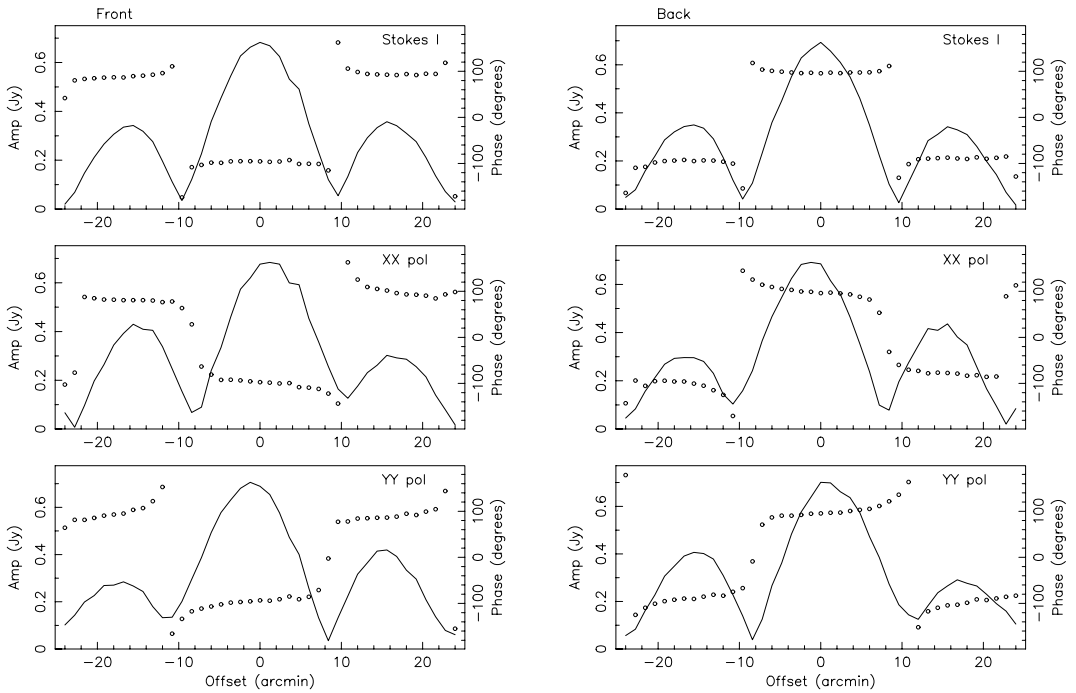

Figure 6. Two antennas 30.6 m apart east–west point nominally towards AZ = 270° and EL = 20°. The variation in amplitude (continuous line) and phase (symbols) of the cross-talk at 4800 MHz are shown as the azimuth of one antenna is offset from the nominal direction keeping the antenna elevation fixed. The panels on the left are for the case where the antenna in front scans in azimuth; those on the right correspond to the case where the antenna at the back scans. The three panels on either side separately show the Stokes *I* visibilities and the *XX* and *YY* polarization products.

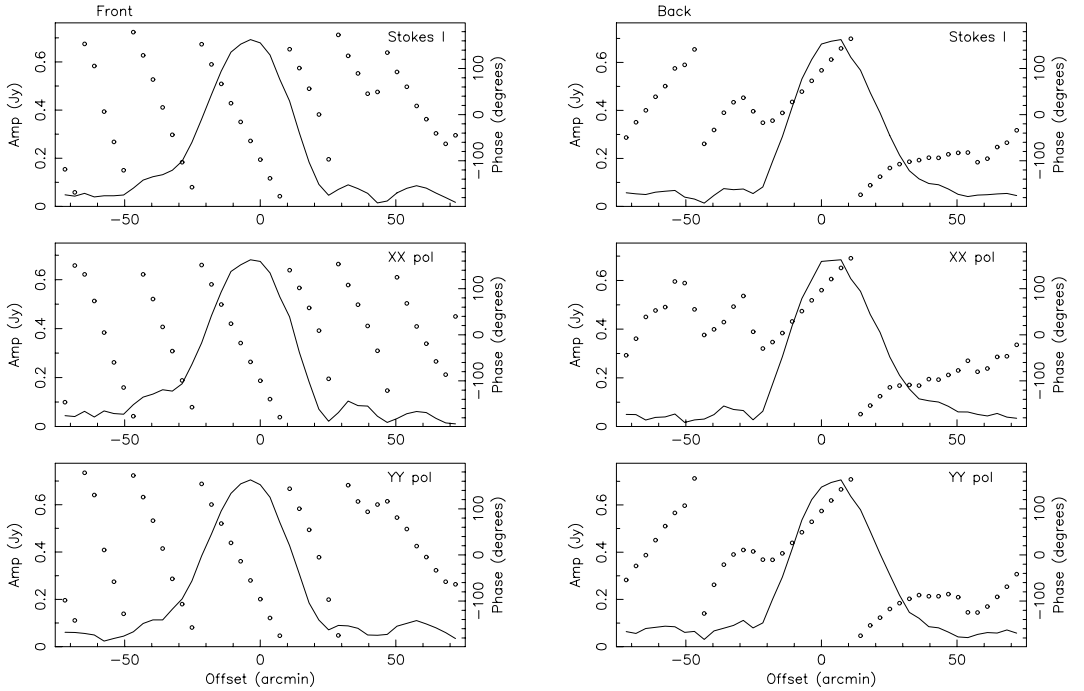

Figure 7. As in Fig. 6, with offsets now applied in elevation instead of azimuth. Both antennas point towards a constant AZ of 270° and the offsets are made in elevation about the nominal EL = 20°.

to that of the stationary antenna (pointing towards the nominal direction); this differential phase has had the phase corresponding to the geometric path delay for the nominal pointing direction subtracted.

First, the cross-talk amplitude falls off fairly rapidly when a relative pointing offset is introduced between the shadowing and shadowed antennas. We have derived first-order estimates of the effective aperture size contributing to the cross-talk from the apparent beamwidths of the scan patterns in azimuth and elevation. These estimates suggest that almost the full horizontal extent and only about half of the vertical extent of the physical apertures may be relevant. This in turn suggests that the observed cross-talk is a vector sum of a large number of coupling paths and that introducing relative pointing offsets between the antennas result in phase distributions across these contributions causing cancellations in the vector summation. The coupling is via multiple paths that are distributed over the aperture; however, the arguments presented earlier require these paths to be very close in their differential delays.

The Stokes *I* azimuth scan patterns are remarkably symmetric and the same (except for the phase sign change) irrespective of whether the antenna in front or that behind is offset from the nominal pointing. The *XX* and *YY* polarization products, for this case where the offsets are made in azimuth, are not only asymmetric but are also shifted in that the peak response occurs at positions offset from the nominal pointing direction. However, they have the symmetry property in that the cross-talk measured in the *XX* polarization product for a positive azimuth offset is the same as the cross-talk measured in the *YY* product for a negative offset. Comparing the scan patterns observed in Stokes *I*, *XX* and *YY* for the two cases where the front antenna scans and where the antenna behind scans, the cross-talk amplitude and phase observed for positive offsets to the front antenna are the same as the cross-talk observed for negative offsets to the antenna at the back. In other words, when each pair of scans for a given product (Stokes *I*, *XX* or *YY*) is viewed as a function of the relative azimuth offset with respect to the pointing of a fixed reference dish, say, of the front antenna, the scan amplitude profiles are the same irrespective of which dish-pointing was offset, while the phase profiles change sign. And the profiles in *XX* are the same as for their *YY* counterparts, except for the flip of the azimuth-offset axis.

The elevation patterns (Fig. 7) do not share many of the symmetry properties of the azimuth scans. First, we observe only marginal differences between the patterns in Stokes *I* and in the *XX* and *YY* polarization products. All the patterns are asymmetric. Additionally, the cross-talk amplitude, in Stokes *I* as well as in the *XX* and *YY* polarizations, peak at a pointing offset from the nominal; i.e. the cross-talk peaks for an antenna configuration in which the front and back antennas are slightly offset in their relative elevation pointings. The elevation scan patterns share a symmetry property with the azimuth scans in that the cross-talk amplitude for positive elevation offsets applied to the front antenna is the same as that for negative offsets to the back antenna. Stated differently, the scan amplitudes (for Stokes *I*, *XX* or *YY*) are about same, irrespective of which dish-pointing was offset, and only depend on the differential pointing, say, of the back antenna with respect to the front antenna. The cross-talk phase patterns in these two cases, however, have very different slopes (versus offset) depending on whether the offsets are made to the antenna at the front or behind.

To summarize the symmetry property common to the azimuth and elevation scans: considering azimuth offsets, the cross-talk is the same irrespective of whether the antenna at the front is offset to the right or the antenna at the back is offset to the left; for elevation offsets, tipping the antenna in front backwards has the same effect on the cross-talk amplitude as tipping the antenna behind forwards. These symmetries are despite the fact that the antenna at the back is shadowed and only a part of its aperture would be illuminated by radiation incident from the pointing direction. The implication is that the cross-talk signal couples from one antenna to the other, so that the cross-talk depends only on the relative orientations of the

pair of antennas: the cross-talk is not a coupling of radiation from an external source independently into the apertures of the two antennas. The common-mode signal probably originates in the antenna in front, couples as a constant signal into the receiver of the front antenna, and propagates across space into the receiver of the antenna behind via the reflectors of that antenna.

It may be noted here that we adopt the convention that the visibility phase ϕ_{ab} of any baseline vector from antenna a to antenna b is the phase corresponding to the differential delay: the delay experienced by the signal arriving at antenna b minus the delay experienced by the signal arriving at antenna a. Therefore, the negative slope in the phase of the antenna in front with respect to the antenna at the back, as the antenna in front is moved up in elevation (panels on the left in Fig. 7), and the positive slope in the phase of the antenna at the back (panels on the right in Fig. 7), imply that the cross-talk signal couples between the apertures of the two antennas via the upper parts of the antenna in front and the lower parts of the antenna at the back.

5.2 A two-dimensional analysis of the distribution in the cross-talk

To investigate further, the offsets to the front and back antennas were made to cover a two-dimensional (2D) grid of azimuth and elevation positions: elevation offsets covered the range $\pm 1\overset{\circ}{.}3$, azimuth offsets covered the range $\pm 1\overset{\circ}{.}235$. These offsets were made to one of the antennas at a time, while the other had its pointing fixed towards the nominal AZ $= 270^\circ$, EL $= 20^\circ$ direction. Complex visibilities, calibrated in Jy, were recorded at each pointing offset. The visibilities were recorded, simultaneously, at 4800 and 8640 MHz and in all the four polarization products, *XX*, *YY*, XY and YX. It may be noted here that the calibrations in amplitude and phase were made using an unresolved source and towards a sky direction where there was no geometric shadowing. The 2D grid of complex visibilities, which were a function of relative sky angles (radians), were then Fourier transformed to produce a complex grid of field distribution estimates, which are distributed in the conjugate variable, that is spatial coordinates with units of wavelengths. The spatial coordinates following the transforms at each frequency were converted to units of metres using the appropriate wavelength.

In Fig. 8 we show the spatial distribution of the field amplitudes that were obtained by a Fourier transformation of the Stokes *I* visibilities recorded at 8640 MHz; we display the field distributions computed via transformations of the complex visibilites recorded while the front antenna executed a 2D raster in azimuth–elevation coordinates and, separately, while the antenna at the back executed the same scan pattern. Before the transformation to spatial coordinates, the visibilities were tapered using a Hamming window. Consequently, the field distribution in spatial coordinates have a point spread function (PSF) with full width at half maximum (FWHM) 1.4 m at 8640 MHz; the side-lobes of the PSF are less than 1 per cent of the peak.

There is considerable fine structure in the correlation amplitude distributions. It may be noted here that most of the structure observed in the amplitude distributions shown in the two panels of Fig. 8 are genuine and have a high significance statistically: the lowest contours plotted are at five times the standard deviation of the image noise. The distribution obtained from the visibilities recorded while the front antenna scanned has a striking similarity, even in details, to the distribution for the case where the back antenna executed the raster scan. Both these images were constructed from independent visibilities, observed at different times, but between the same pair

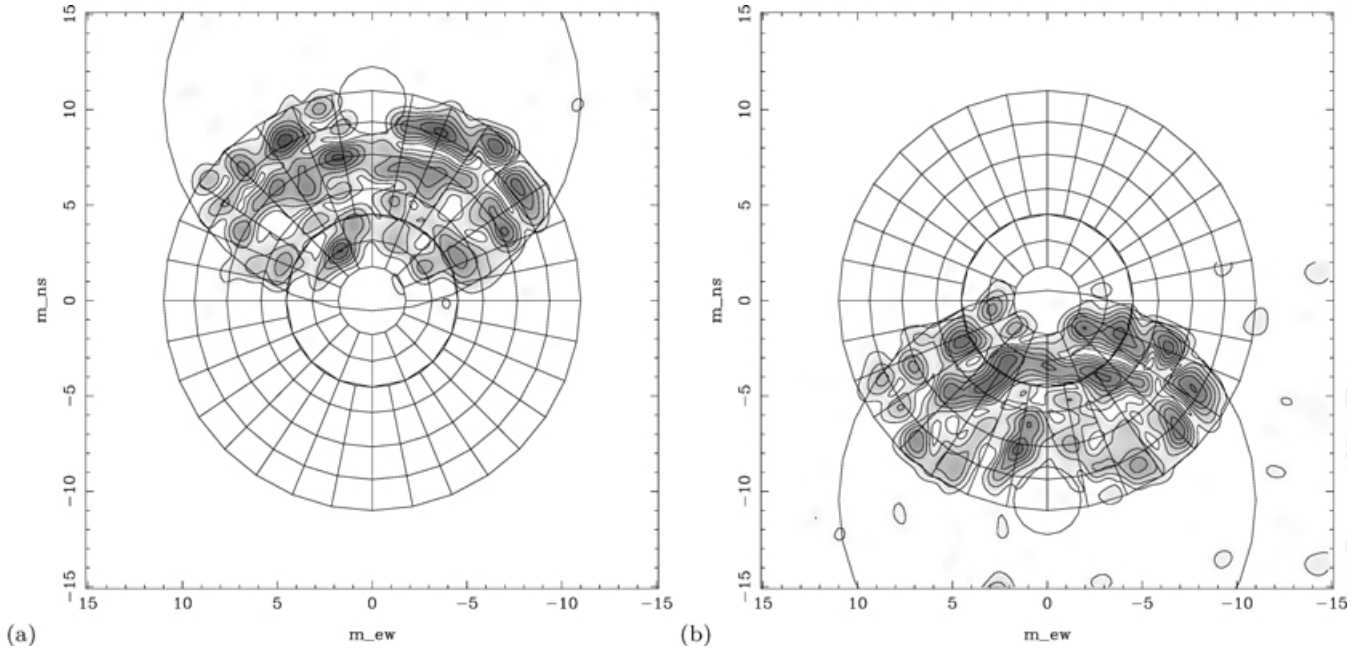

Figure 8. The 2D Fourier transformation of the distribution in cross-talk over antenna pointing. The measurements are in Stokes *I* and at 8640 MHz. In the case of the panel on the top, the visibilities input to the transform were acquired while the front antenna executed a 2D raster in azimuth and elevation while the antenna at the back pointed towards the nominal AZ $= 270^\circ$, EL $= 20^\circ$ direction. The panel at the bottom corresponds to the case when the back antenna executed the raster scans. The panels show the distribution in the transform amplitude and the plot coordinates are in units of metres. On the top panel, a grid showing the layout of the panels of the antenna in front is overlaid, and the outer and inner limits of the panels of the antenna at the back are also shown; these overlays are projections perpendicular to the nominal pointing direction. On the bottom panel, the layout of the back antenna panels and the outline of the front antenna aperture are overlaid. Contours are at 15, 30, 45, 60, 75 and 90 per cent of the peak; the rms noise is at a level of 3 per cent of the peak.

of antennas and with the same antenna in front at both times. The similarity in the details of the distributions is additional confirmation that the observed structure is well above the image noise.

The Stokes *I* distribution does not show any obvious relationship to the panel structure, but does show a clear correspondence with the concentric annular structure of the front dish. For example, there are nulls in the amplitude distribution at specific radii measured from the vertex (centre) of the aperture of the front antenna. In the 8640-MHz data, the nulls are located at radial distances of 5.5 and 8.7 m and at these radii the phase flips by about 180°. At 4800 MHz, a phase flip is observed at a radius of 4.6 m. It may be noted here that the detailed structure in the distribution has been observed to differ when the measurements are made using a different pair of antennas. The overall distribution is observed to vary also with frequency.

The holographic imaging of the cross-talk confirms and extends many of the inferences derived from the azimuth and elevation scan data. First, it may be inferred that the cross-talk does not arise due to a coherent wavefront incident on the antenna pair from the far field and parallel to the pointing direction. If this were the case, the 2D Fourier transforms of the cross-talk visibilities that were recorded while the two antennas separately executed azimuth/elevation scans would have given us images of the entire aperture for the case where the front antenna scanned and images of the unblocked aperture for the case where the shadowed antenna scanned. Additionally, the cross-talk is not a consequence of the scattering by the front antenna, of power from a plane wavefront that is incident on the front antenna, to the second antenna behind.

The Fourier transforms of the 2D azimuth/elevation raster scans, made separately for the antenna in front and the antenna behind (see Fig. 8), are the same. This is consistent with the interpretation in which the common-mode signal enters one of the antennas – the antenna in front – as a constant coupling independent of the small variations in the azimuth/elevation pointing of that antenna during the raster scan. This common-mode signal is radiated by elements of that antenna and couple into the aperture of the antenna behind. The distribution of the field sharply cuts off at the edges of the overlap region. The cross-talk field is also zero in the central regions of the two apertures that are occupied by the feed housing at the vertices of the main reflectors. The holographic imaging indicates that the cross-talk coupling is localized to the segments of the apertures that would appear to overlap as viewed from the direction towards which the antennas point; the coupling is confined to the areas of the apertures that geometrically shadow. Additionally, it rules out any transverse coherence in the coupling field on scales more than a small fraction of the aperture (i.e. more than a few Fresnel scales). The similarity in the distributions derived from data in which the front antenna scanned and that in which the back antenna scanned indicates a one-to-one correspondence between points on the front and back antenna apertures; the common-mode field might be viewed as propagating from the front antenna aperture to the back antenna aperture along lines parallel to their optical axes. Additional evidence for such a propagation path is the observation that the signal enters the receivers with a relative delay that is the same as that for a celestial source in the direction that the antennas point. A coupling via propagation between the overlap portions of the two apertures is consistent with the observations that the variations in cross-talk visibility only depend on the relative pointing between the two antennas and that the two Fourier transforms in Fig. 8 display the same distribution.

The images in Fig. 8 show that the signal arrives at the back antenna exclusively from the region of the back surface of the front antenna that shadows the antenna behind. In other words, the common-mode signal propagates to the aperture of the back antenna from the entire back surface of the front antenna. Given that the Fresnel scale is small (less than 2 m), the power associated with the cross-talk can be considered as propagating more or less along lines parallel to the optical axis of the back antenna and will reach the receiver of that antenna after reflections off the main and subreflectors of that Cassegrain antenna. As viewed by the antenna behind, the source of the common-mode signal is in the main reflector surface of the antenna in front.

If the source is mainly spatially incoherent emission distributed across the surface of the main reflector of the antenna in front, the observation that the cross-talk appears at zero lag (after the geometric path delay corresponding to the pointing direction is removed) once again leads to the inference that the emission must couple across the main reflector surface in a distributed manner.

5.3 The distribution in the polarization of the cross-talk

The symmetry properties of the scan data, in Stokes *I* as well as in the polarization products, and the images of the distribution in the field amplitude across the aperture suggest that the cross-talk coupling between the two antennas is described via a single coupling distribution: the measurements made by scanning the antenna in front or the antenna at the back are both a measurement of the same coupling field. To investigate the polarization in this coupling, we have examined the distributions in the aperture field of the *XX* and *YY* polarization products. In Figs 9 and 10 we show these distributions, at 4800 and 8640 MHz, respectively, for the case where the front antenna executed the raster scan. The complex visibility data that were transformed to produce these images were not tapered and, therefore, in the case of the distribution at 8640 MHz displayed in Fig. 10, the spatial resolution is about a factor of two better as compared to the corresponding Stokes *I* distribution shown in Fig. 9; however, the PSF now has higher side-lobes. The polarization images at 8640 MHz (Fig. 10) have a PSF resolution that is about a factor of two finer than that for the polarization images at 4800 MHz (Fig. 9). These polarization product images represent the cross-talk field distribution projected on the antenna apertures and the view is of the antenna apertures face on. In this face-on view, the *XX* linear polarization corresponding to the feed is oriented at a position angle of -45° and the *YY* polarization is at $+45^\circ$ with respect to the vertical.

Both of the *XX* and *YY* polarization images have distributions that cover the entire overlap segment. There is a wealth of detailed structure in the field distribution across the aperture. The most striking aspect is that the structures appear elongated: (i) the elongations in each of the images are orthogonal to the orientation of the feed polarization, and (ii) the elongated structures show a remarkable correspondence with the panel edges. At both frequencies, the *XX* polarization images show enhanced brightness along the radial interpanel gaps on the left halves of the overlap sectors whereas the *YY* polarization images show enhanced brightness along the radial interpanel gaps on the right halves of the overlap sectors. At 8640 MHz, the *XX* polarization image shows enhanced emission along the circumferential interpanel gaps in the right half of the overlap segment and the *YY* polarization images shows enhanced emission along the circumferential interpanel gaps in the left half of the overlap segment. At 4800 MHz, the emission in the right half of the *XX* polarization image and the left half of the *YY* polarization image are diminished at the interpanel gaps and appear to be peaked at the panel centres. It may be noted here that this correspondence is

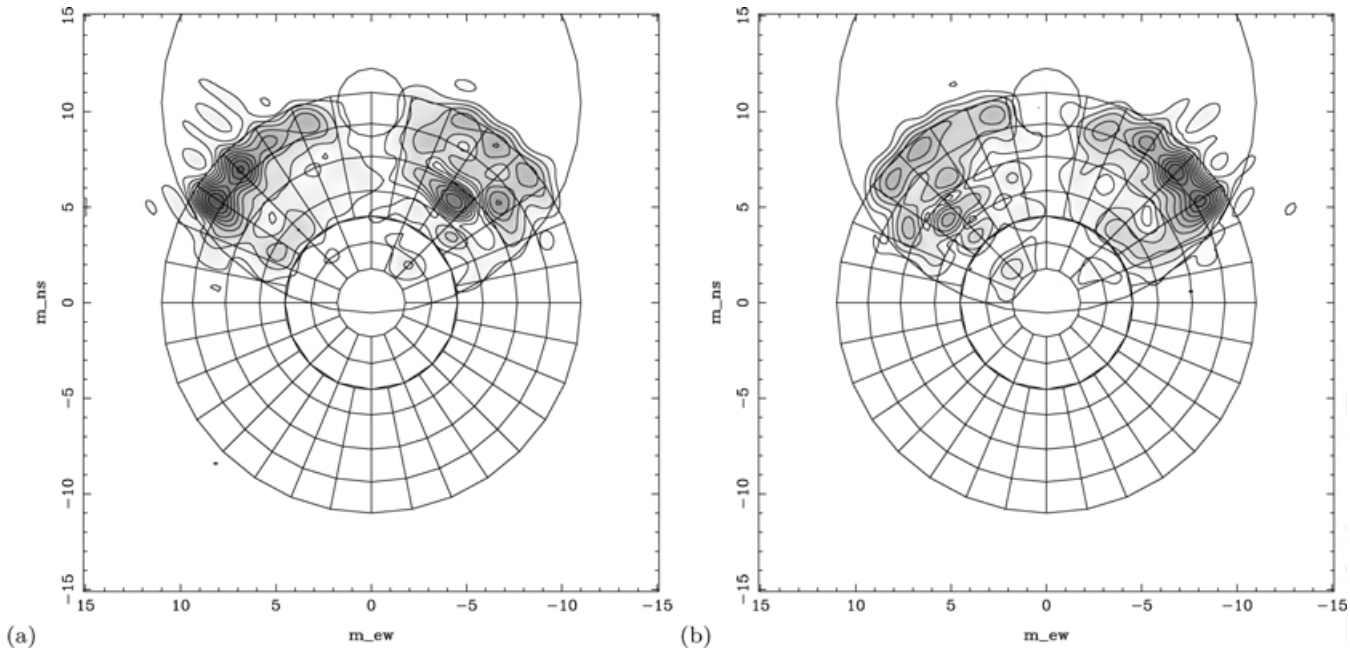

Figure 9. The 2D Fourier transformations of the *XX* (top panel) and *YY* (bottom panel) polarization product measurements of the cross-talk at 4800 MHz. In both cases, the visibilities input to the transform were acquired while the front antenna executed a 2D raster in azimuth and elevation while the antenna at the back pointed towards the nominal AZ = 270°, EL = 20° direction. The panels show the distribution in the transform amplitude and the plot coordinates are in units of metres. A grid showing the layout of the panels of the antenna in front is overlaid, and the outer and inner limits of the panels of the antenna at the back are also shown. Contours are at 10, 20, 30, 40, 50, 60, 70, 80 and 90 per cent of the peak.

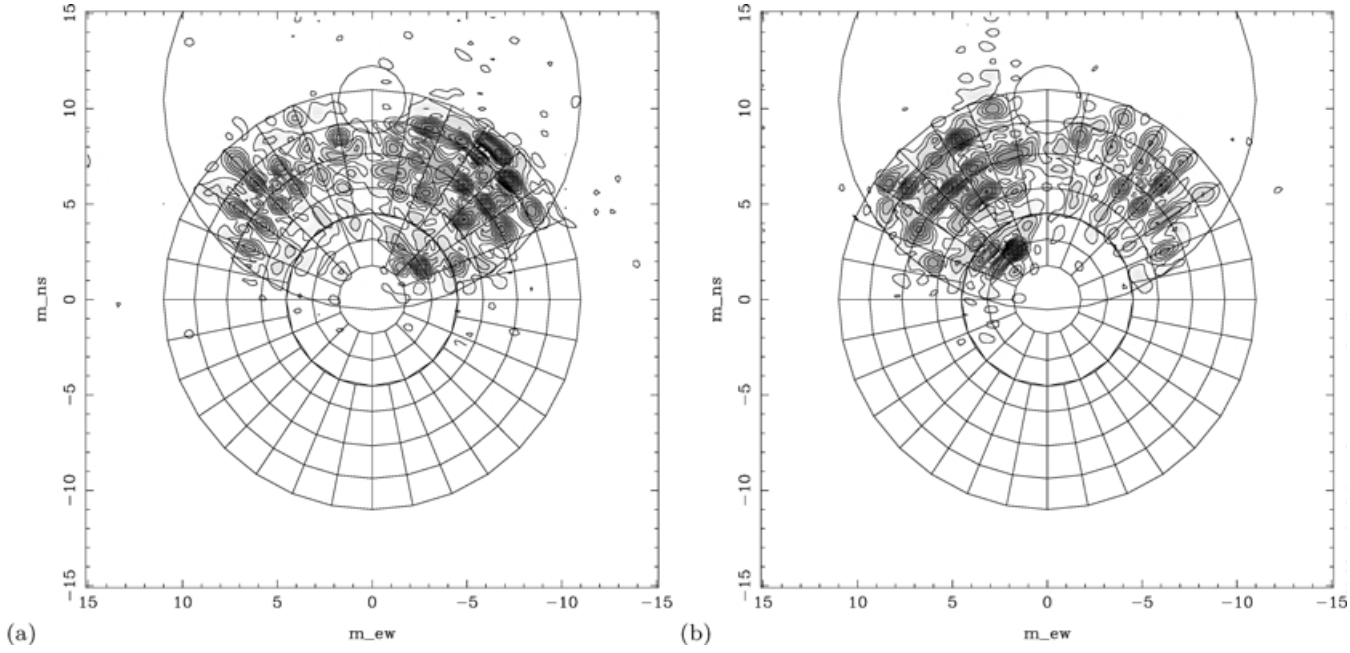

Figure 10. The 2D Fourier transformations of the *XX* (top panel) and *YY* (bottom panel) polarization product measurements of the cross-talk at 8640 MHz. The coordinates, contour intervals and labelling are as in Fig. 9.

with the layout of the front antenna panels, not those of the antenna behind, consistent with our earlier inference based on the Stokes *I* images.

A slot between the plates that form a reflector surface may couple radiation across the surface, or act as a slot antenna; the resulting emission will be linearly polarized with an orientation perpendicular to the slot. Such radiation, with polarization perpendicular to panel edges (i.e. panel gaps) and that perpendicular to the slots (within the panels), will be picked up by polarization products that are oriented perpendicular to the panel edges and slots. This is what is observed in Figs. 10 and 11. The polarization images suggest that the polarization products respond to cross-talk associated with those panel edges/gaps/slots that are oriented orthogonal to the feed polarization orientation. In the images made at 8640 MHz (Fig. 10), the *XX*

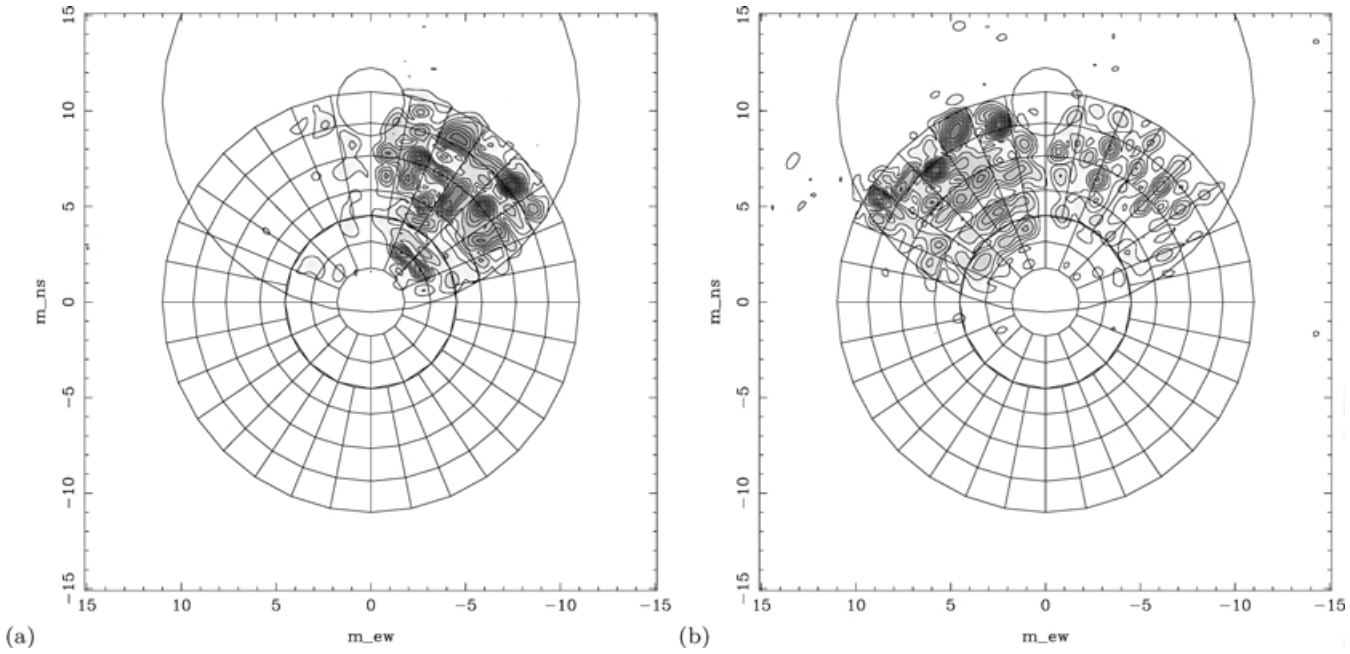

Figure 11. Same as Fig. 10 except that in this case the interpanel gaps in a quarter of the front antenna were sealed with aluminium foil tape. In this face-on view of the antenna apertures, the tape covered the gaps in the top-left quarter of the front antenna.

polarization product (corresponding to -45° PA) appears to respond to radiation from the circumferential edges of the panels in the right half of the overlap segment and radial edges of the panels in the left half of the overlap segment. The *YY* polarization product, which is oriented orthogonal to the *XX* product and at a PA of $+45^\circ$, picks up radiation from the other sets of edges/slots. The dominant source of the cross-talk radiation, at 8640 MHz, appears to be linearly polarized emission that couples into the receivers from the interpanel gaps distributed over the part of the front antenna main reflector that geometrically overlaps the antenna behind.

It may be noted here that there appears to be significant emission, in the right half of the *XX* polarization and the left half of the *YY* polarization images at 8640 MHz, that are off the circumferential interpanel gaps. Additionally, at 4800 MHz, the emission in these regions appears centred on the panels. These imply that a significant cross-talk component, with a linear polarization oriented circumferentially, does originate away from the interpanel gaps and from the panels themselves.

The main reflector panels are bolted to the backup structure and there are gaps of about 1–2 mm between the solid panels. In order to examine whether the cross-talk is purely owing to a leakage of radiation through these gaps, we used aluminium tape (3M 425 aluminium foil tape) to seal all the interpanel gaps over one quarter of the main reflector of the antenna in front; with the front antenna viewed face on, all interpanel gaps in the the entire upper left quadrant were covered. The aluminium tape was stuck on over the paint; however, the tape would be expected to provide electrical continuity at the observing frequency. Raster scans were executed with the aluminium tape stuck on. Fig. 11 shows the results for this case: the aperture field distributions obtained as Fourier-transform images of the *XX* and *YY* polarization products at 8640 MHz. It may be noted here that the antenna pair used for this measurement was not the same as the pair used for producing Figs 8 or 10.

The most striking effect of the aluminium tape is that the cross-talk aperture field, in the quadrant where the tape was stuck on, is not detectable in the *XX* polarization product. The *YY* polarization product detects significant emission from the aperture region where the interpanel gaps were sealed; however, the image of the field in this region is different as compared to the case without the tape in that the distribution does not follow the circumferential gaps between the panel rings. Instead, with the tape sealing the gaps, the cross-talk field appears to avoid the panel boundaries. The experiment with the aluminium tape confirms the inference that the coupling of radiation across the main reflector surface is not wholly due to the interpanel gaps. There is an additional component distributed over the panel surfaces; this surface component is linearly polarized with an *E*-field oriented in the radial direction.

The ATCA panels are solid surfaces; however, as mentioned in Section 3, they are not constructed from single metal sheets. The panels are made of circumferential segments that are riveted on to I-section backup ribs. Before assembly, a layer of epoxy resin was applied to the rib so that the panels could take on the shape of the assembly mould – a bed of bolts – without stresses on the stretch-formed ribs. The epoxy serves as a gap filler and this manufacturing process allows gaps between the panel surfaces and the backup ribs. We observe that the surface component has a polarization perpendicular to the slits between the sheets forming the panels just as the edge component has a linear polarization perpendicular to the gaps between the panels. It appears that the intrapanel slits between the panel sheets, in addition to the interpanel gaps between panels, are both associated with the cross-talk.

At 8640 MHz, the distributions in Fig. 10 show that overall the *XX* amplitude is greater in the right half of the segment whereas the *YY* amplitudes are greater on the left side. We observe that in the lower-frequency observations, at 4800 MHz, the *XX* amplitudes are greater in the left side and the *YY* amplitudes are greater on the right side, which is the opposite of what is observed at 8640 MHz. At 4800 MHz, the intrapanel component, with a polarization oriented radially, dominates the cross-talk in the right-half segment of the *XX* polarization and the left-half segment of the *YY* polarization.

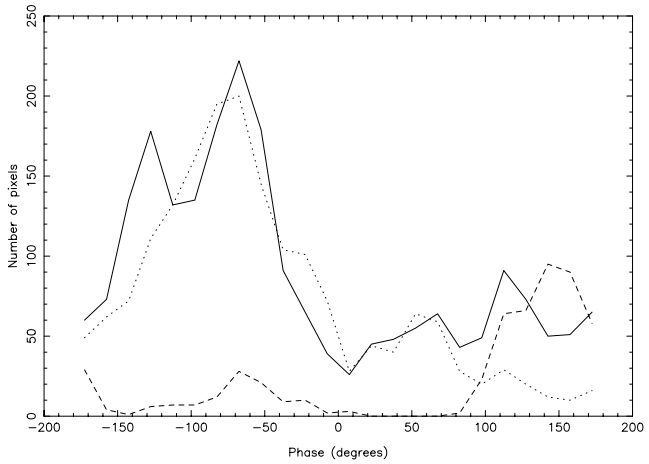

Figure 12. Histograms of the observed phase distributions – at 8640 MHz – across the aperture in the case where the interpanel gaps in a quadrant of the front antenna aperture was covered with aluminium tape. The continuous line shows the histogram of the *XX* polarization phases in the right half of the face-on aperture (the top panel in Fig. 11). The dotted line shows the *YY* polarization phases in the left half of the aperture (the bottom panel in Fig. 11); the dashed line shows the *YY* polarization phases in the right half of this aperture.

In these regions, this intrapanel contribution dominates that arising from the circumferential interpanel gaps. At the higher frequency of 8640 MHz, the intrapanel contribution is subdominant. These comparisons between the images in Figs 9 and 10 indicate that the relative dominance of the intra- and interpanel contributions, the relative strengths of the cross-talk signal arising from the radial and circumferential interpanel gaps, and also the radial variation in their individual strengths, are significantly dependent on wavelength, at least at centimetre wavelengths.

5.4 The phase associated with the components of the cross-talk

The histograms in Fig. 12 show the distribution in the observed phases in the case where the upper left quadrant (face-on view) of the front antenna had aluminium tape covering the interpanel gaps. The phases in the right half of the *YY* polarization image, shown using a dashed line, correspond to the phase of the cross-talk arising from the radial interpanel gaps and show a peak at about $+150^\circ$. The phases in the left half of the *YY* polarization image, shown using a dotted line, correspond to the phase of the cross-talk arising from the intrapanel slits and peak at about -70°. The histogram of the phases in the right half of the *XX* polarization image, shown as a continuous line, corresponds to phases of the cross-talk signal from intrapanel slits and circumferential interpanel gaps; this histogram is seen to be a combination of the dotted and dashed histograms indicating that here we have a bimodal distribution and that the cross-talk arising from the radial and circumferential interpanel gaps have similar phases. The histogram distributions imply that there are different phases associated with the cross-talk arising from the inter- and intrapanel slots and that they are both very different from that expected for a point source at the interferometer phase centre. The intrapanel slits have I-section backup members running along the slits on the backsides of the panels; the interpanel gaps also have structural members running along the gaps. Therefore, there is no direct line-of-sight that is parallel to the optical axis and from the slits or gaps to the aperture plane of the antenna behind. These structural backup members may be responsible (at least in part) for the observed phases associated with the contributions from the gaps and slits. It may also be noted here that the observed phases for the different cross-talk contributions vary with the observing frequency. The observed phase differences and the frequency dependance may be related to the path delays owing to scattering off the backup structure; as discussed in Section 4, such a path delay of a few centimetres is expected from the observed variation in the phase of the cross-talk over a decade in frequency.

6 A MODEL FOR THE CROSS-TALK

We have attempted to construct a model for the cross-talk. A face-on view of the ATCA antenna main reflector, showing the interpanel gaps and the intrapanel slits, is in Fig. 13. All of these gaps and slits are modelled as sources of spatially incoherent broad-band thermal radiation. With a pair of antennas 30.6 m apart, pointing nominally at an azimuth of 270° and elevation of 20°, and in a configuration with geometric shadowing, the emission from the front side of the main reflector surface is picked up by the receiver of the antenna in front after a single reflection off its subreflector; emission from the back surface propagates to the receiver of the antenna behind after reflections off its main and subreflectors. The model assumes that at any point along the gaps and slits, the radiation emerging from the two sides of the front antenna main reflector is coherent although spatial incoherence is assumed along the gaps and slits.

The signal received by the front antenna, from the distributed source on its main reflector surface, is a constant that is independent of the antenna pointing. Radiation from the back surface was propagated to the aperture plane of the antenna behind using a physical optics (PO) approximation; these signals propagated across space to the receiver of the antenna behind after reflections off the main and subreflectors of the antenna behind. The propagation to the receiver of the antenna behind involved an additional reflection as compared to the propagation to the receiver in the front antenna and, consequently, were phase shifted through an additional π radians. The lack of spatial coherence in the emission from the surface was accounted for in the modelling by computing the correlated response of the interferometer for each element of the surface emitter separately and then vectorially summing over the responses. When both antennas point towards the same sky direction and their optical axes

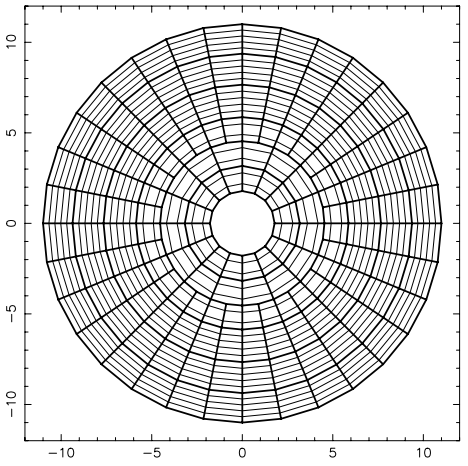

Figure 13. A face-on view of the ATCA antenna main reflector showing the layout of the panels. The boundaries of the panels are shown with thicker lines; these are the lines along which the interpanel gaps lie. The intrapanel slits are shown using lighter lines. The plot axes are in metres.

are parallel, the path lengths of the GO rays, from every element of the surface of the main reflector of the shadowing antenna to the receivers on the front and back antennas, are identical. However, in the GO approximation, the response to this emission will have a phase of π radians owing to the additional reflection off the main reflector of the back antenna. In the PO approximation, the phase differs from π radians even when the optical axes of the two antennas are parallel and the interferometer visibility phase depends on the shadowing geometry.

The emission associated with the gaps and slits was assumed to be 100 per cent polarized on both sides of the surface, and the *E*-field of the radiation is assumed to be oriented perpendicular to the gap/slit. The model allowed for a differential weighting to be applied to the emission from the intrapanel gaps relative to the interpanel slits. The model also allows for constant phase terms to be added to the radiation from the back surface of the main reflector; the value of this phase is allowed to be different for the gaps and slits. The weighting may be physically associated with the relative intensities of radiation from the gaps with respect to the slits; the phase terms may be physically associated with the extra propagation paths for the back-propagating rays because their direct lines of sight to the back antenna aperture are blocked by backup structural elements. The blockage owing to the legs of the tetrapod supporting the subreflector was modelled by omitting those rays that are incident on any of the two antenna apertures within sectors of 10° angles centred at the locations of the legs. Additionally, the Fresnel diffraction at the tetrapod legs was modelled by a down-weighting of the rays that were incident within 20° sectors centred at the locations of the legs. The PO computation was made of the interferometer response, with a pair of antennas spaced 30.6-m apart and pointing nominally at AZ $= 270^\circ$, EL $= 20^\circ$ and with pointing offsets made in azimuth and elevation to the antenna in front and behind; the offsets were made to only one of the antennas at any time while the other continued to be pointed at the nominal position. The goal of this modelling was to examine whether the observed scan patterns shown in Figs 6 and 7 could be reproduced with reasonable choices for the parameters of the model.

First, the computation confirms that the observed scan patterns are broadly reproducible with the source modelled as spatially incoherent emission distributed over the entire surface of the front antenna main reflector. In the shadowed configuration being considered here, the individual polarization products (*XX* and *YY*) respond to emission associated with inter- and intrapanel circumferential slots in one half of the overlap segment and interpanel radial slots in the other half. Introduction of a differential phase term between the intrapanel slits – which are all circumferential – and the interpanel gaps, results in the polarization products responding to emission that has a net phase variation across the length of the overlap segment. When one of the antennas in the shadowed configuration is scanned in azimuth, this phase difference causes the *XX* and *YY* polarization responses to peak at locations offset from the nominal pointing. Indeed, this is what is observed in Fig. 6 and the modelling reveals that a differential phase of about 60° between the gaps and slits reproduces these shifts as well as the asymmetries in these polarization product scan patterns at 4800 MHz. At 8640 MHz, the modelling suggests a phase difference of about 160°. The modelling at 4800 MHz required that the emission, per unit length, from the intrapanel gaps be weighted up relative to that from the intrapanel slits: we have used a relative weighting factor of four for the computation at this frequency. An overall radial weighting was implemented by weighting up the components distributed over the outermost ring of panels by a factor of two as compared to that from the inner rings.

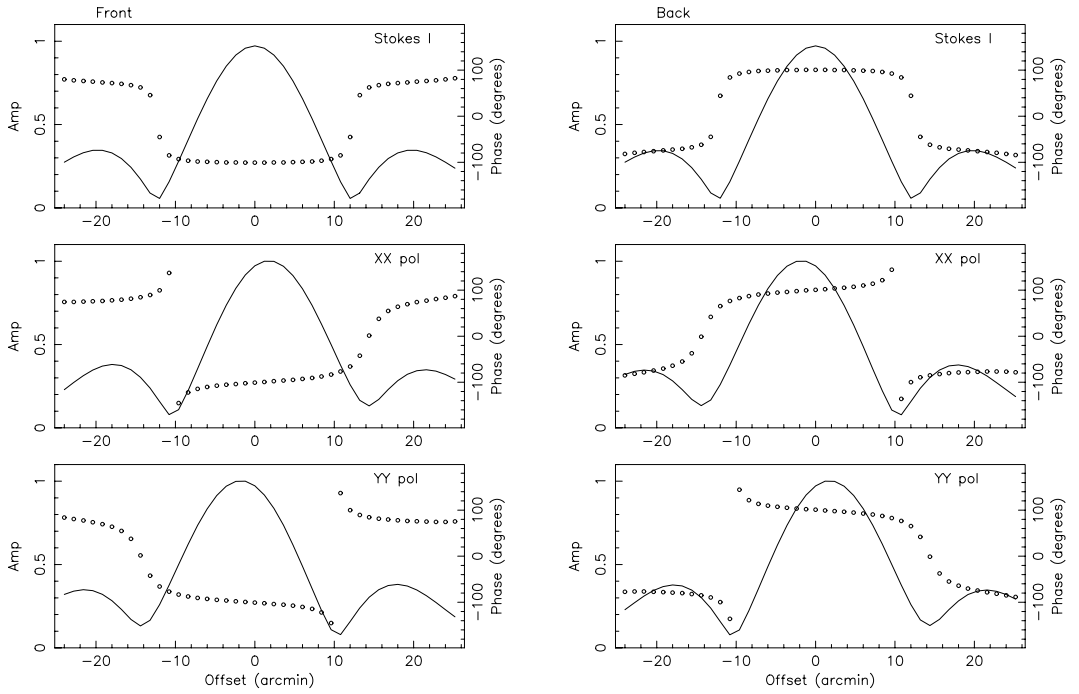

Figure 14. The computed cross-talk amplitudes and phases, in Stokes *I* as well as in the *XX* and *YY* polarization products, are shown here assuming that it arises from 100 per cent linearly polarized emission, which is spatially incoherent and distributed along the gaps and slits in the main reflector surface of the antenna in front. Two antennas, which are 30.6 m apart east–west, point nominally towards AZ $= 270^\circ$ and EL $= 20^\circ$. The variation in amplitude (continuous line) and phase (symbols) of the cross-talk at 4800 MHz are shown as the azimuth of one antenna is offset from the nominal direction keeping the antenna elevation fixed. The panels on the left are for the case where the antenna in front scans in azimuth; those on the right correspond to the case where the antenna at the back scans. The three panels on either side separately show the Stokes *I* visibilities and the *XX* and *YY* polarization products.

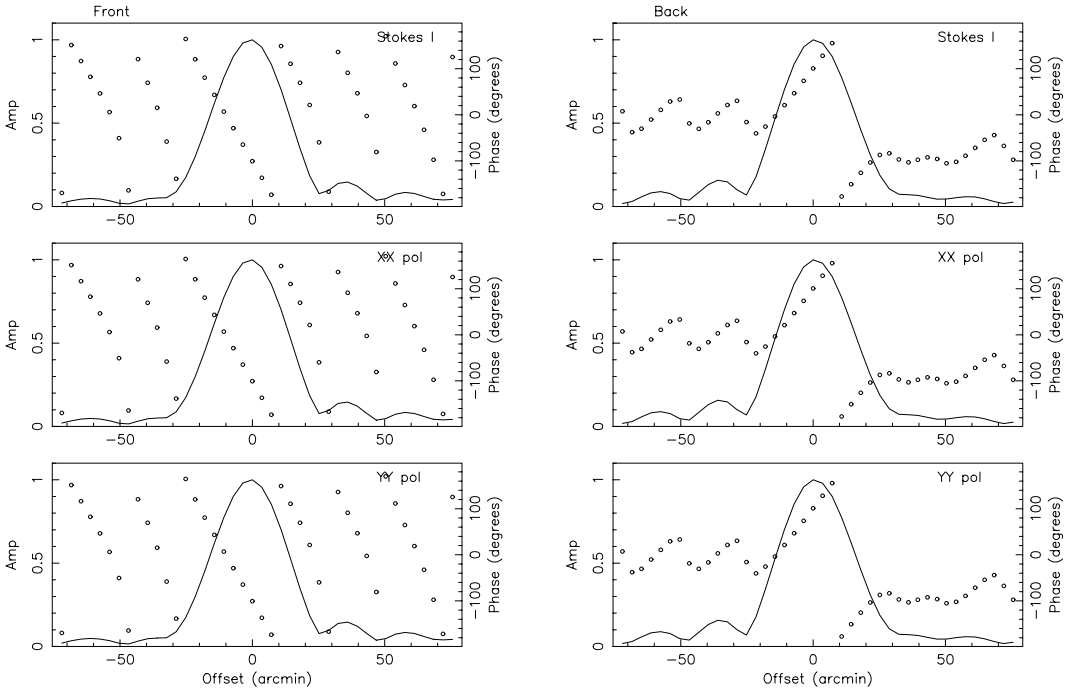

Figure 15. As in Fig. 14, with offsets now applied in elevation instead of azimuth. Both antennas point towards a constant azimuth of 270° and the offsets are made in elevation about the nominal EL = 20°.

The computed amplitudes and phases of the cross-talk, in Stokes *I* and in the *XX* and *YY* polarization products, versus pointing offsets in azimuth and elevation, are shown in Figs 14 and 15. The scan patterns, computed for the model, agree with the observations in most respects suggesting that we have a good model for the cross-talk. It is indeed remarkable that we have been able to successfully model the high-side-lobe azimuthal scans, the shifts and asymmetries in the *XX* and *YY* polarization product azimuth scans, the elevation scan patterns along with the asymmetries in their side-lobe structure and the different phase patterns observed in the elevation scans when the antennas at the back and front were separately scanned. It may be noted here that the PO computation was important for the modelling (as opposed to a GO approximation); in particular, the PO analysis was essential for reproducing the asymmetries in the elevation scan patterns.

There are some aspects of the observed scans that have not been reproduced very well and we believe that these details might depend on, for example, the detailed understanding of the frequency dependence of the radiative properties of the slots and gaps on the antenna surface, the interaction of the back-propagating radiation with the backup structural members and the variation in this interaction with radius. Another aspect that we have not addressed in the modelling is the possibility of partial spatial coherence in the emission across the surface of the main reflector of the antenna in front.

7 COMMENTARY

The cross-talk arises because of coherence in the emission, associated with the interpanel gaps and intrapanel slits, from opposite sides of the main reflector of the antenna in front. The ATCA reflectors are constructed from aluminium sheets and the skin depth for centimetre-wavelength radiation is about 1 μm and any electromagnetic (EM) field would drop exponentially to insignificant values as it propagates through the panels. Therefore, any cross-talk of the kind we observe at the ATCA cannot arise from radiative propagation through the solid panels and requires a coupling conduit across the panel surfaces. Our examination of the nature of the cross-talk, particularly its polarization characteristics, clearly show that interpanel gaps and, more surprisingly, intrapanel slits, can serve as the cause for coherence in the emission from the opposite sides of the reflector surface.

The incident EM field from the sky, with an intensity corresponding to the sky brightness, has a partial spatial coherence due to the large-scale brightness temperature variations on the sky. The ATCA receiver has a circulator in the signal path between the feed horn and the first low-noise amplifier; the circulator has a third port terminated by a load that is cooled to cryogenic temperatures and the brightness of the subreflector, as viewed by elements of the main reflector, corresponds to the physical temperature of this load. Elements of the front surfaces of the panels of the antenna that is in front receive radiation from the background sky as well as from the subreflector. In a configuration where an antenna geometrically shadows another, the back surfaces of the panels (of the antenna in front) see the sky reflected off the antenna behind and also see the ground along other lines of sight. All these incident fields are potentially primary sources for the currents on the panel surfaces. The gaps and slits might be lines along which currents couple across the panel surfaces causing coherence in surface currents and, consequently, coherence in the secondary emission from currents on the panel surfaces. It may be recalled here that the observations described in Section 4.1, showing that the cross-talk amplitude depends only of the length of the projected shadowed baseline and may be the same at different antenna elevations and when the shadowed segments are at different regions of the main reflector surface, argue against ground re-radiation from the slots as a possible mechanism for the cross-talk.

All the panels of the main reflectors are in thermal equilibrium with the surrounding air that is at ambient temperature. The panel surfaces are spatially incoherent emitters of their thermal heat; however, because of their high reflectivity the emissivity of the

aluminium panels is small and corresponds to a brightness temperature of not more than a few kelvin. As discussed above, this radiation from opposite sides of the solid panel surfaces would not be expected to be coherent and, therefore, would not result in cross-talk if they are picked up by different elements of an interferometer. Gaps and slits in the panel surfaces would, however, act as slot antennas and these would emit EM radiation, that is coherent, when viewed from opposite sides of the surface. Stochastic voltages are induced across the gaps and slits corresponding to the physical temperature of the panels and the efficiency of the slot antenna would depend on its geometry and its impedance match to free space.

We finally attempt an understanding of the observed strength of the cross-talk. At 4800 MHz, when the projected baseline is 13 m and the antennas are separated by 30.6 m, the cross-talk signal is measured by the ATCA correlator to have a correlation coefficient of 0.075 per cent. The geometric mean system temperature of the antenna pair in this shadowed configuration is about 60 K implying that the cross-talk corresponds to an antenna temperature of 45 mK. In this configuration, where the antennas point towards an elevation of 25°, the area of geometric shadowing is 112 m^2. The area of geometric shadowing is 30 per cent of the area of the main reflector and this implies that the emission from the main reflector surface, which is received by any one of the antennas, has a mean brightness temperature of 150 mK. We may account for this level of radiation, together with the observation that the cross-talk amplitude scales inversely with frequency, if we assume that the slots act as radiators with an effective temperature that is 1–2 per cent of the physical temperature (about 300 K), and an effective area that corresponds to the slot length times a width that is one wavelength. The first assumption might be related to the 98–99 per cent reflectivity of the surface metal; the second aspect might be related to the fact that a thin slot (or dipole) antenna has an effective area (as a receiver or radiator) that has a width of the order of one wavelength. In such a case, the slots would have an effective area that is about 3 per cent of the reflector surface at 4800 MHz.

It is interesting to ask whether all of the additive cross-talk, in interferometer baselines with geometric shadowing, could be eliminated by designing the antennas to be made of solid surfaces. A possible mechanism for cross-talk in this case is scattering/emission of common-mode power from those parts of the outer rim of the front antenna that overlap the antenna behind. However, in shadowed configurations, our measurements of the distribution of the cross-talk across the aperture show no cross-talk component associated with the outer rim of the main reflector surface of the antenna in front (see Figs 10 and 11).

8 SUMMARY

The nature of unwanted spurious signals seen in ATCA baselines in shadowed configurations has been examined. This cross-talk appears to be a linearly polarized additive component which arrives at the receivers of both antennas with almost exactly the delay that a celestial source would have if it were at the pointing centre.

Our examination of the cross-talk signal and its variation with the shadowing configuration indicates that the spurious interferometer response is a result of emission from the main reflector surface of the antenna in front. Coherence between the emission from the front and back surfaces of this reflecting surface, which propagate respectively into the receivers of the antennas in front and at the back, result in an interferometric response, as observed. The coherence is due to the gaps between the panels forming the main reflector surface as well as slits between the plates that are bonded together to form the panels. We conclude that this mode of cross-talk may be avoided in short-spacing interferometers by constructing the main reflector surfaces as continuous conducting sheets. In the present case, thin conducting stripes (like aluminium tape) covering all the gaps would reduce considerably the cross-talk between the ATCA dishes in shadowed configurations. Alternately, this cross-talk would be avoided if the backside of the main reflector is covered with conducting sheets.

ACKNOWLEDGMENTS

The Australia Telescope is funded by the Commonwealth of Australia for operation as a National Facility managed by CSIRO.

REFERENCES

Bennett J. C., Anderson A. P., McInnes P. A., Whitaker A. J. T., 1976, IEEE Trans. Antennas Propagat., 24, 295
Birkinshaw M., 1990, in Mandolesi N., Vittorio N., eds, The Cosmic Microwave Background, 25 Years Later. Kluwer, Dordrecht, 77
Carlstrom J. E., Joy M. K., Grego L., Holder G. P., Holzapfel W. L., Mohr J. J., Patel S., Reese E. D., 2000, Phys. Scripta, T, 85, 148
Church S. E., 1995, MNRAS, 272, 551
Jones M. et al., 1993, Nat, 365, 320
Lay O. P., Halverson N. W., 2000, ApJ, 543, 787
Padin S., Cartwright J. K., Joy M., Meitzler J. C., 2000, IEEE Trans. Antennas Propagat., 48, 836
Ryle M., 1962, Nat, 194, 517
Ryle M., Hewish A., Shakeshaft J. R., 1959, IRE Trans. Antennas Propagat., 7, 120
Scott P. F., Ryle M., 1977, MNRAS, 178, 539
Subrahmanyan R., 2002, in Chen L.-W., Ma C.-P., Ng K.-W., Pen U.-L., eds, ASP Conf. Ser. Vol. 257, AMiBA 2001: High-z Clusters, Missing Baryons, and CMB Polarization. Astron. Soc. Pac., San Fransisco, p. 309
Sunyaev R. A., Zeldovich Ya. B., 1972, Comm. Astrophys. Space Phys., 4, 173

This paper has been typeset from a TEX/LATEX file prepared by the author.